Meteorol Atmos Phys 86, 261–273 (2004)
DOI 10.1007/s00703-003-0025-z

Meteorology and Atmospheric Physics
Printed in Austria

[1] Center for Climate Systems Research, Earth Institute at Columbia University, NASA/Goddard Institute for Space Studies, New York
[2] Stinger Ghaffarian Technology, Inc., NASA/Goddard Institute for Space Studies, New York

Land surface influences on the West African summer monsoon: Implications for synoptic disturbances

L. M. Druyan[1], **M. Fulakeza**[1], and **P. Lonergan**[2]

With 12 Figures

Received February 23, 2003; accepted April 22, 2003
Published online: January 28, 2004

Summary

The study examines regional atmospheric model (RM) simulations of the mean June–September (JJAS) climate and the implications of the mean state for the model representation of African wave disturbances (AWD). Two simulations are made with a version of the RM that computes soil moisture with multivariate functions that statistically relate it to rainfall, surface temperature, albedo, vegetation and terrain slope. These simulations differ according to the assignment of ground temperatures (Tg). While the control experiment is based on the fully interactive computation of soil moisture, the second experiment tests the response to fixed Tg whose seasonal means are more realistic than in the control within a swath along the Gulf of Guinea coast. A third simulation is made with the RM coupled to a sophisticated land surface process model (RM2). Results show a rather acute sensitivity of the mean circulation to land surface processes. The more realistic meridional temperature gradient created by fixing Tg in turn increased the vertical wind shear over West Africa and eliminated unrealistic westerly circulation at 700 mb. AWD composites were transformed from intense closed cyclonic circulations with copious rainfall to more realistic open waves that organized more moderate precipitation maxima. Lower vorticity variances in the specified change experiment imply that the open waves were characterized by more moderate vorticity extremes. Corresponding spectral amplitudes for 3–6 day periodicities of the 700 mb meridional wind were 40–80% of control values within the swath of maximum AWD activity. From among the three simulations, RM2 achieved seasonal mean precipitation, temperature, energy flux and circulation distributions that, despite some unrealistic features, were closest to observational evidence. RM2 AWD were much less intense and favored slightly longer periods. Results demonstrate that discrepancies in modeled ground temperatures caused by underestimating the cloudiness that intercepts short wave solar flux along a narrow swath of the West African coast have far-reaching consequences for the simulation of both the mean summer climate and individual synoptic disturbances. The study implies that this cooling along the Gulf of Guinea coast prevents AWD from developing into more intense storms with heavier precipitation.

1. Introduction

The evolution of the rainy phase of the West African monsoon during early summer controls the northward advance of seasonal rainfall into the Sahel. Drought conditions are often associated with abbreviated northward incursions of the inter-tropical convergence zone during years with positive sea-surface temperature (SST) anomalies in Southern Hemisphere oceans (especially the South Tropical Atlantic) and negative SST anomalies north of the equator (Lough, 1986; Folland et al, 1986; Lamb and Peppler, 1992). Alternatively, it is possible that negative precipitation anomalies over the Sahel are also a consequence of diminished frequencies or

diminished intensities of African wave disturbances (AWDs), but the evidence is not conclusive. The role of AWDs has been studied empirically (Druyan et al, 1996; Taleb and Druyan, 2003) and with atmospheric model simulations (Druyan and Hall, 1996; Druyan, 1998).

Typical AWD wavelengths are about 2500 km (Burpee, 1972), but convergence zones, vertical motion extremes and squall lines are often confined to one wave sector (Reed et al, 1977). We have previously documented the performance of the NASA/Goddard Institute for Space Studies (GISS) regional model (RM) over West Africa during a two-week period in August 1988 (Druyan et al, 2001) (hereafter DFLS). The RM exploits the relatively high resolution 0.5° grid spacing of a limited area atmospheric model in order to better analyze the spatial structure of meteorological fields associated with synoptic features over West Africa. The model domain, 20° S–35° N, 35° W–35° E, includes the region of AWD formation in the eastern Sahel, the region of cross-equatorial flow in the Gulf of Guinea, the entire Sahara and Atlantic coastal waters. DFLS showed realistic RM mid-tropospheric circulation and precipitation simulations forced by ECMWF observational analyses as lateral boundary conditions.

Characteristics of AWDs relate to the mean atmospheric state, and especially to the configuration of the African Easterly Jet (Thorncroft and Blackburn, 1999). The present study examines the RM simulation of the mean June–September (JJAS) climate and its implications for AWDs. In particular, a rather acute sensitivity of the results to land surface processes is elucidated.

2. The model and experiments

The RM1 version of the regional atmospheric model used in previous published studies is described by DFLS. It solves the primitive equations on 15 sigma surfaces using a semi-lagrangian advection scheme and semi-implicit time differencing. The treatment of long and short wave radiation transfer includes diurnal and seasonal variations, absorption by greenhouse gases and interactive clouds. Terrain topography is specified at 0.5° resolution, consistent with the horizontal computing grid. Fulakeza et al (2002) explain the model's land surface (LS) scheme whereby soil moisture is computed interactively by second-order regression equations that are functions of simulated rainfall, albedo, surface temperature, normalized difference vegetation index (NDVI) and terrain relief. LS albedo evolves during the simulation according to variations in soil moisture, following Deardoff (1978).

The version referred to below as RM2 shares the same atmospheric model with RM1, but it is coupled to a LS process model based on the scheme used in the GISS GCM (Rosenzweig and Abramopoulos, 1997). This LS component replaces the multivariate functions of RM1 for computing soil moisture. Considerable experience with the LS model in the GISS GCM (Hansen et al, 2002) and more recent testing with the RM2 have demonstrated its utility, showing a reasonable agreement of results with observational evidence.

The present study is based on two June–September simulations with RM1 and a single parallel simulation with RM2. In each case, synchronous NCEP reanalysis (NCPR) data interpolated from six-hourly records from 1 June–30 September 1995, are used as lateral boundary data to drive RM1 or RM2. These data include observed SST which also define the regional model's lower boundary conditions over ocean points. Since RM1 and RM2 are driven by observational data in these experiments, the simulations characterize a downscaling of NCPR to the finer resolution represented by the 0.5° grid. The second RM1 simulation tests the impact of a swath of prescribed invariant ground temperatures along the Gulf of Guinea coast, as explained below.

3. Results

3.1 RM1 control experiment, JJAS means

Figure 1a shows the JJAS 1995 cross-section of RM1 temperatures in the lower troposphere along 0° longitude over West Africa and the Gulf of Guinea. Figure 1b shows the corresponding cross-section based on NCPR data. A comparison suggests that the RM1 near-surface Saharan temperature maximum is not high enough, while the temperature gradient southward toward the Gulf of Guinea is underestimated. RM1 temperatures along the Gulf of Guinea coast are several

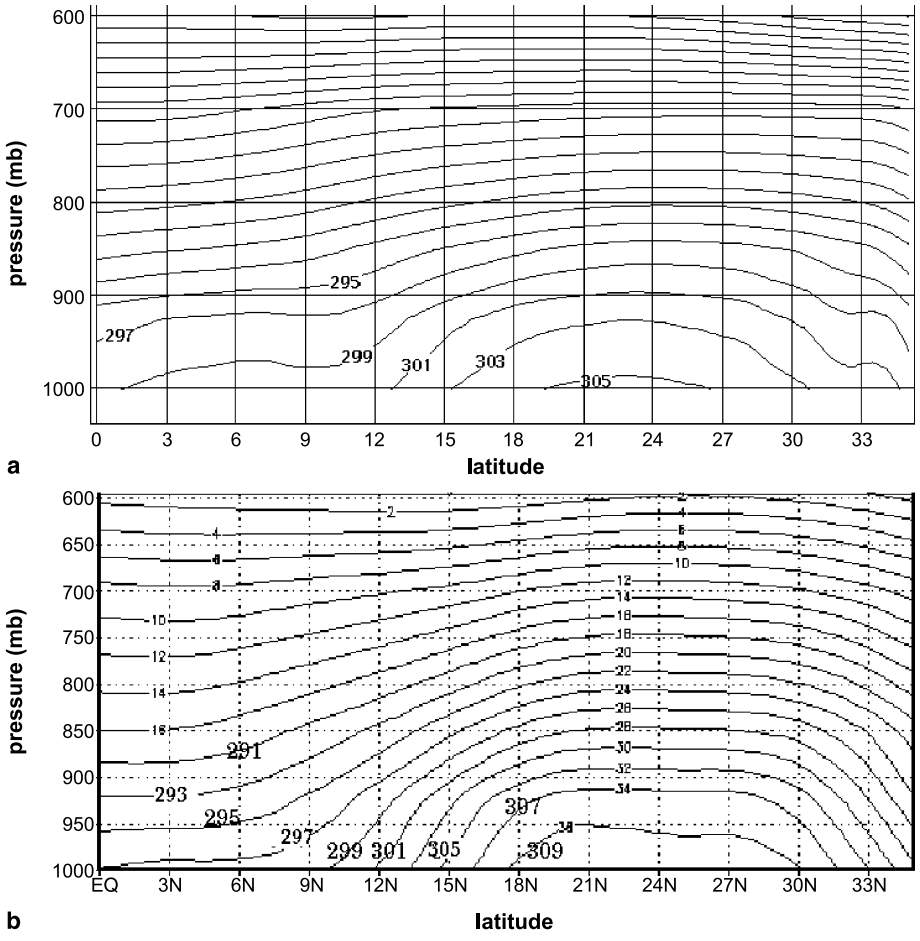

Fig. 1. Latitude-pressure cross-sections of temperature (K) along 0° longitude; **a** Regional model simulation, control, **b** NCEP reanalysis data (courtesy CDC/NOAA)

degrees too high, possibly related to unrealistic model deficits of precipitation and/or inaccuracies in the surface energy balance. The diminished meridional temperature gradient implies a weakened westerly directed thermal wind which in this example generates only about 70% of the NCPR- analyzed negative zonal wind shear over West Africa.

Figure 2a is the JJAS 1995 cross-section of RM1 zonal wind speeds, also along 0° longitude. Modeled monsoon westerlies at lower levels are much too strong. Moustaoui et al (2002) also reported unrealistically strong monsoon westerlies over West Africa in their GCM simulations spanning 14 summers. They speculated that such discrepancies may reflect limitations in a model's treatment of land surface processes. For this JJAS 1995 simulation, the immediate problem relates to the RM1 SLP distribution which concentrates too much of the pressure gradient along the Gulf of Guinea coastal region. Comparison of Fig. 2a and b indicates that the mid-tropospheric African Easterly Jet is only slightly weaker than analyzed, but it is displaced about 5° northward. The RM1 monsoon westerlies correctly weaken with altitude, but since the near-surface circulation is so strong, even a realistic negative wind shear allows the zonal circulation to remain positive within a rather deep layer. This weakens the AEJ over 10–15° N, while negative wind shear atop a stalled zonal circulation closer to 18° N forms a jet core above 700 mb. Figure 3 shows that this RM1 circulation pattern creates a narrow zone of strong lateral wind shear at 700 mb oriented southeast to northwest. Note that the configuration of the AEJ affects AWD trajectories and probably intensities. These waves are most intense near the jet level and are therefore steered by the mean mid-tropospheric circulation. Moreover, energy for AWD development is derived from lateral and vertical wind shear near the AEJ (Thorncroft and Blackburn, 1999).

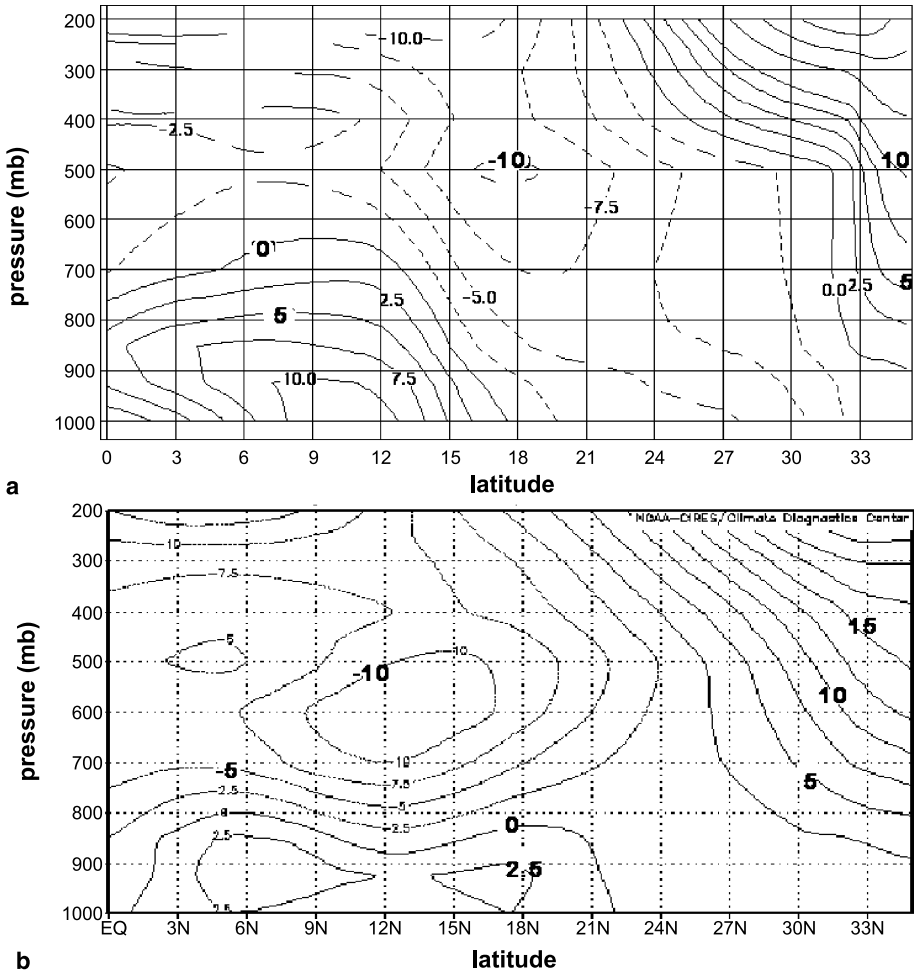

Fig. 2. Latitude-pressure cross-sections of zonal wind (ms^{-1}) along 0° longitude; **a** Regional model simulation, control, **b** NCEP reanalysis data (courtesy CDC/NOAA)

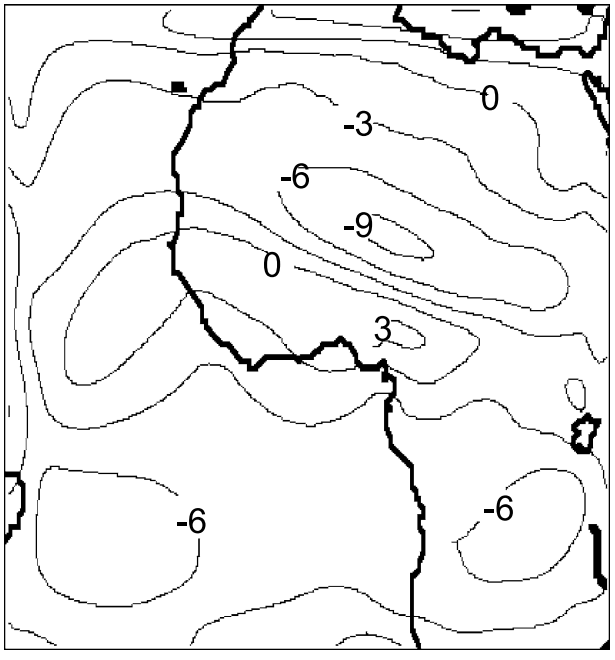

Fig. 3. Zonal wind speeds (ms^{-1}) at 700 mb for the regional model simulation, control

Pytharoulis and Thorncroft (1999) associated AWD at 700 mb with the shear south of the AEJ core.

Figure 4a shows the JJAS 1995 mean ground temperatures computed by the RM1. SSTs, prescribed from NCPR data, are also shown. Figure 4b is the corresponding distribution for NCPR data. The diminished meridional temperature gradient over West Africa is the most glaring deficiency of these RM1 results. While the Sahara maximum is well simulated, temperatures along the Gulf of Guinea coast are about 6 K too warm. Since this is a rainy region during JJAS, unrealistic features in simulated ground moisture that have an adverse effect on the surface energy balance are suspected.

3.2 RM1 Tg experiment, JJAS means

An ad hoc experimental simulation was made to test the impact of a more realistic cold tongue

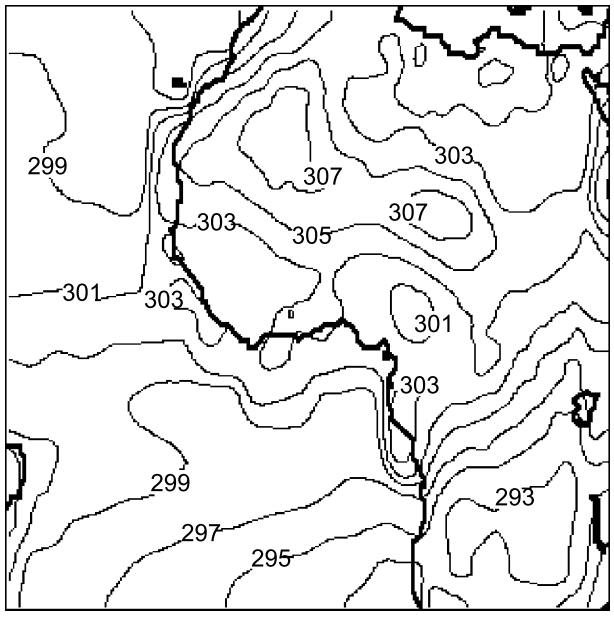

a

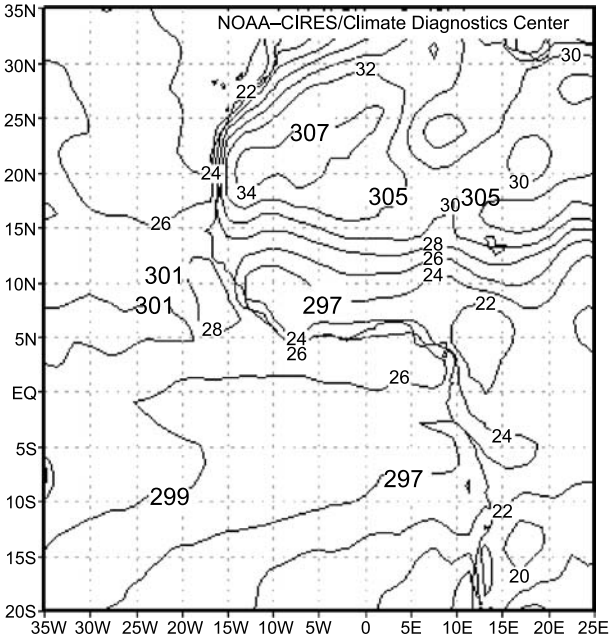

b

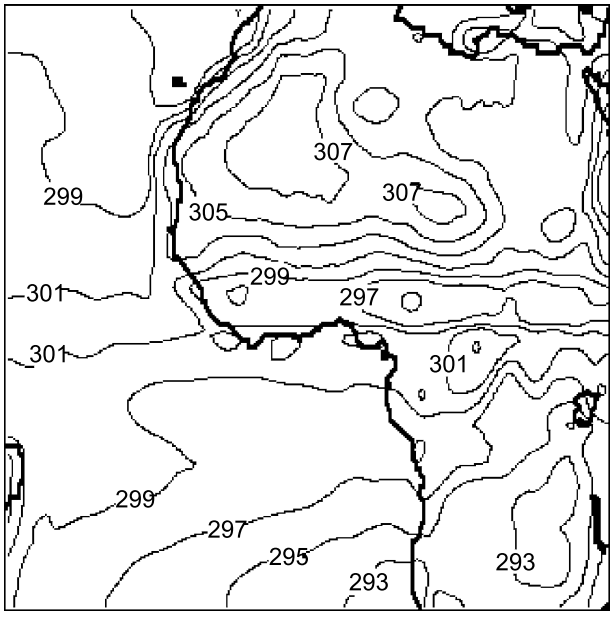

c

Fig. 4. June–September 1995 mean ground temperatures (K); **a** Regional model simulation, control, **b** NCEP reanalysis data (courtesy CDC/NOAA), **c** Regional model simulation with swath of prescribed Tg

along the Gulf of Guinea coast on the simulation. The interactive computation of ground temperature (Tg) was disabled at some 137 grid elements between 6–10° N, 11° W–5° E, where an idealized Tg minimum, compatible with NCPR JJAS mean values (Fig. 4b), was fixed for the entire four-month simulation. These Tg also did not undergo any diurnal cycle variations.

Figure 4c shows Tg for the experiment (hereafter, Tg *experiment*), including the prescribed values at the 137 grid elements and JJAS means computed with the interactive scheme elsewhere over the continent. Figure 5a shows the latitude-pressure cross-section of resulting mean JJAS temperatures along 0° longitude over West Africa and the Gulf of Guinea for this experiment. It is clear that prescribing this cold tongue had the effect of tightening the meridional temperature gradient in the lower troposphere over West Africa compared to the original simulation

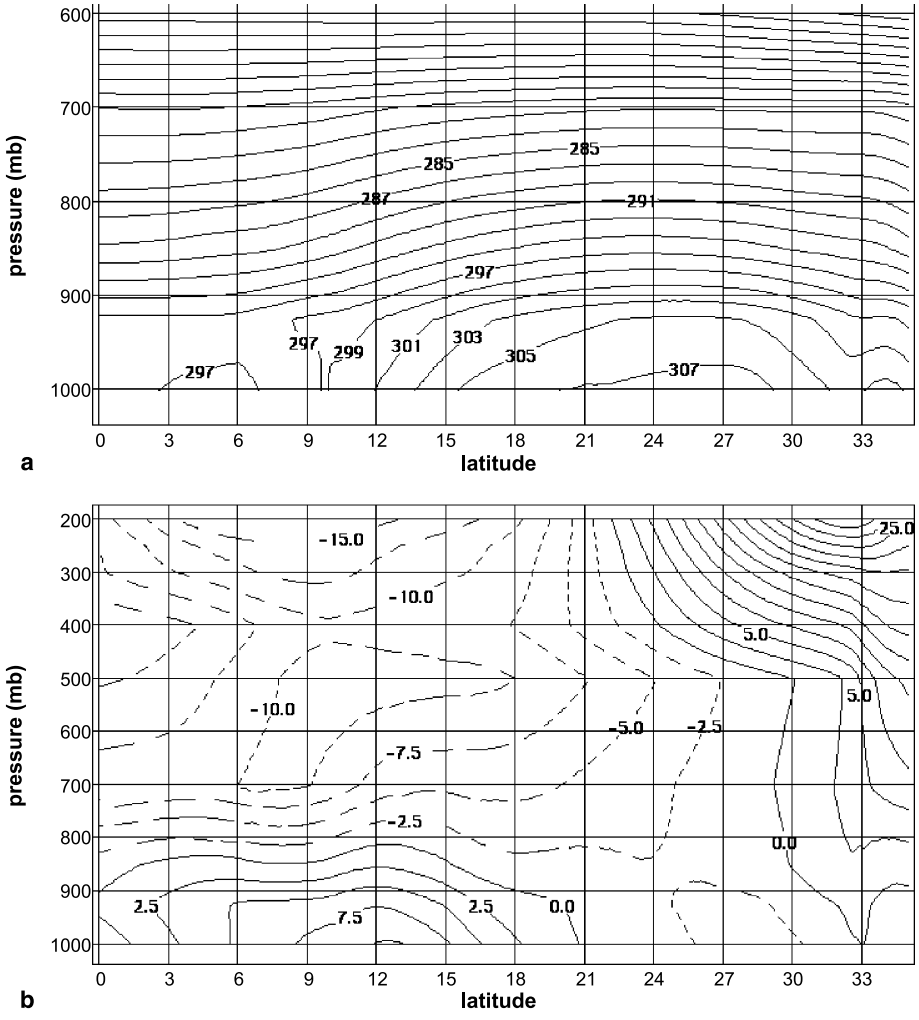

Fig. 5. Latitude-pressure cross-sections along 0° longitude for the regional model simulation with swath of prescribed Tg; **a** temperature (K), **b** zonal wind (ms^{-1})

(Fig. 1a), and of decreasing lower tropospheric temperatures to approximately the correct values over the Gulf of Guinea (Fig. 1b). Moreover, the change had a beneficial impact on the SLP distribution, creating a discontinuity in gradient that is discernable in the NCPR data, thereby causing a modest reduction in the monsoon westerlies in the lowest layers (Fig. 5b). The augmented temperature gradient has also enhanced the negative vertical wind shear making the westerlies much shallower and allowing the zonal wind to reverse to easterlies below 700 mb. This simulation accordingly features a more realistic jet core of easterlies between 700–500 mb, centered along 10° N. At 700 mb (Fig. 6a), the unrealistic streak of westerlies over West Africa apparent in the control (Fig. 3) has been eliminated, although the easterly maximum is displaced about 5° southward of the NCPR AEJ core (Fig. 6b). Some unrealistic features of the experimental simulation results were inevitable since Tg within the designated swath was invariant in this experiment, its normal diurnal cycle was eliminated and daytime peaks were prevented. The unrealistic temperature inversion over 9° N discernable in Fig. 5a is evidence of the negative impact of fixing Tg. This in turn led to a rather complete cessation of local convective rainfall (not shown). The impact of the altered mean state on AWD characteristics is discussed below.

3.3 RM2 experiment, JJAS means

The ad hoc Tg experiment showed improvements in the simulated JJAS circulation over West Africa despite its inherent flaws. Since prescribed Tg within the affected swath were invariant with time, they could not experience the strong diurnal variability of the region and they must also have been generally incompatible with the

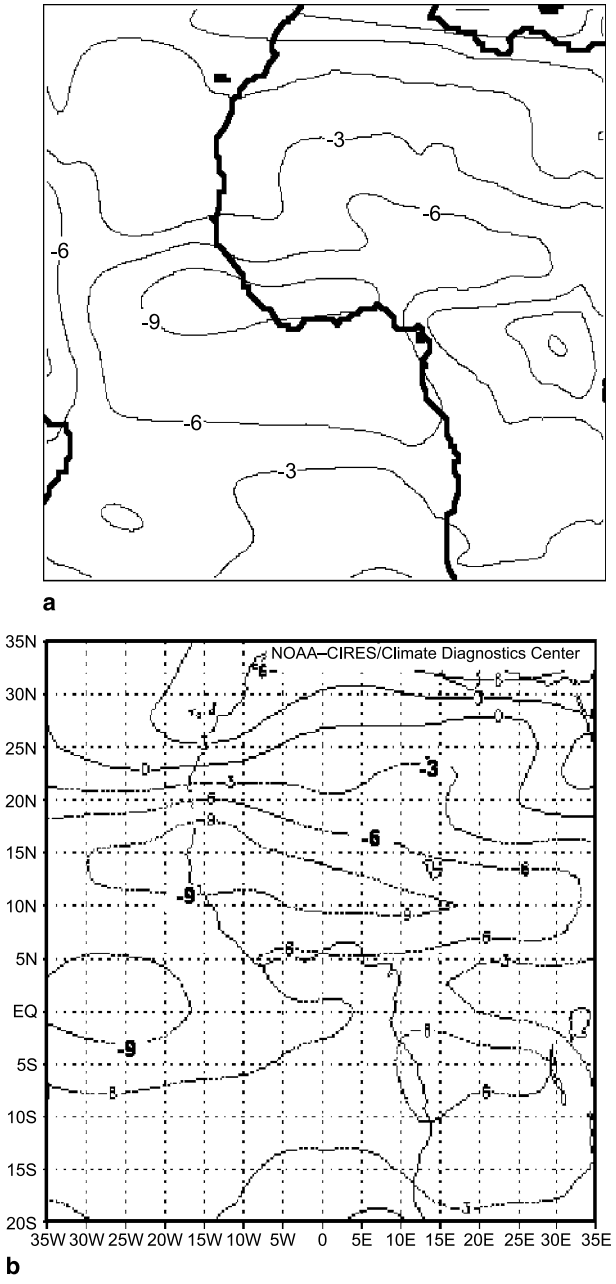

Fig. 6. Zonal wind speeds (ms^{-1}) at 700 mb; **a** Regional model simulation with swath of prescribed Tg, **b** NCEP reanalysis data (courtesy CDC/NOAA)

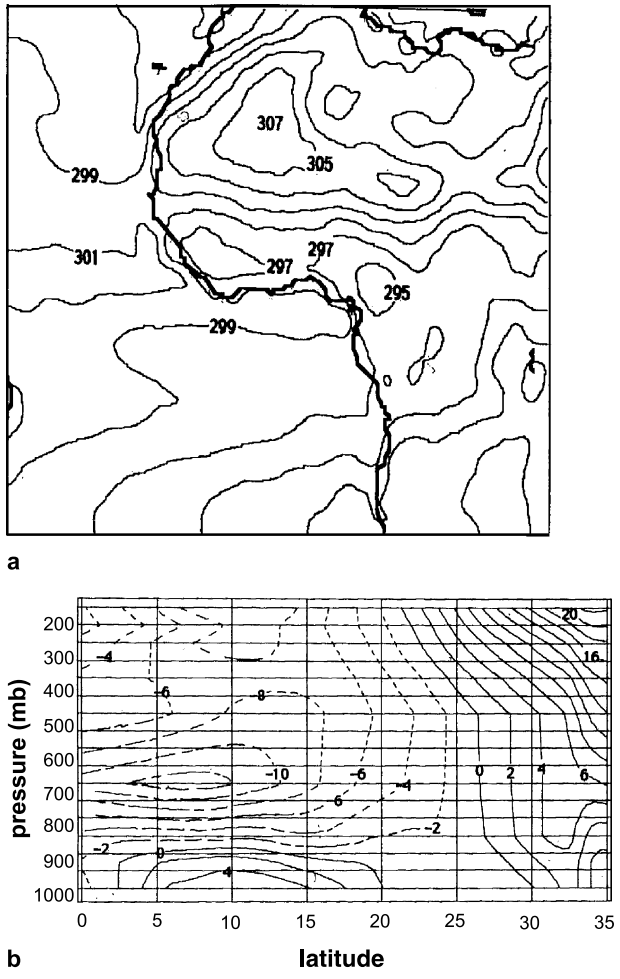

Fig. 7. RM2 JJAS mean fields, **a** Tg, **b** latitude-pressure cross-section of zonal wind (ms^{-1}) along 0° longitude

computed physics. The RM2 offers the possibility to simulate seasonal mean Tg that are more realistic than those of RM1 by means of a fully interactive physical model.

Figure 7a shows the JJAS mean Tg from the RM2 simulation. Comparison with the RM1 result shown in Fig. 4a shows that coupling the RM with the land surface process model has greatly modified the mean Tg parallel to the Gulf of Guinea coast. In fact, these RM2 simulated Tg are now in very close agreement with the corresponding NCRP product. The Sahara maximum is slightly underestimated, but a realistically strong meridional Tg gradient is evident.

Figure 8a shows the JJAS mean distribution of soil moisture for the RM2, expressed as a fraction of saturation. The swath where computed Tg were less than 297 K corresponds to soil moisture fractions that exceed 0.60 and these are the highest over the domain. The same area experiences elevated JJAS mean upward latent heat fluxes (Fig. 8b) that are undoubtedly related to the high soil moisture fraction. Upward sensible heat flux was particularly low for this area (Fig. 8c) and short wave radiation flux received at the surface averaged about 210 Wm^{-2} (Fig. 8d). By way of contrast, the soil moisture fractions for the RM1 control run (Fig. 8e) were lower, exceeding 0.6 only within narrow strips along

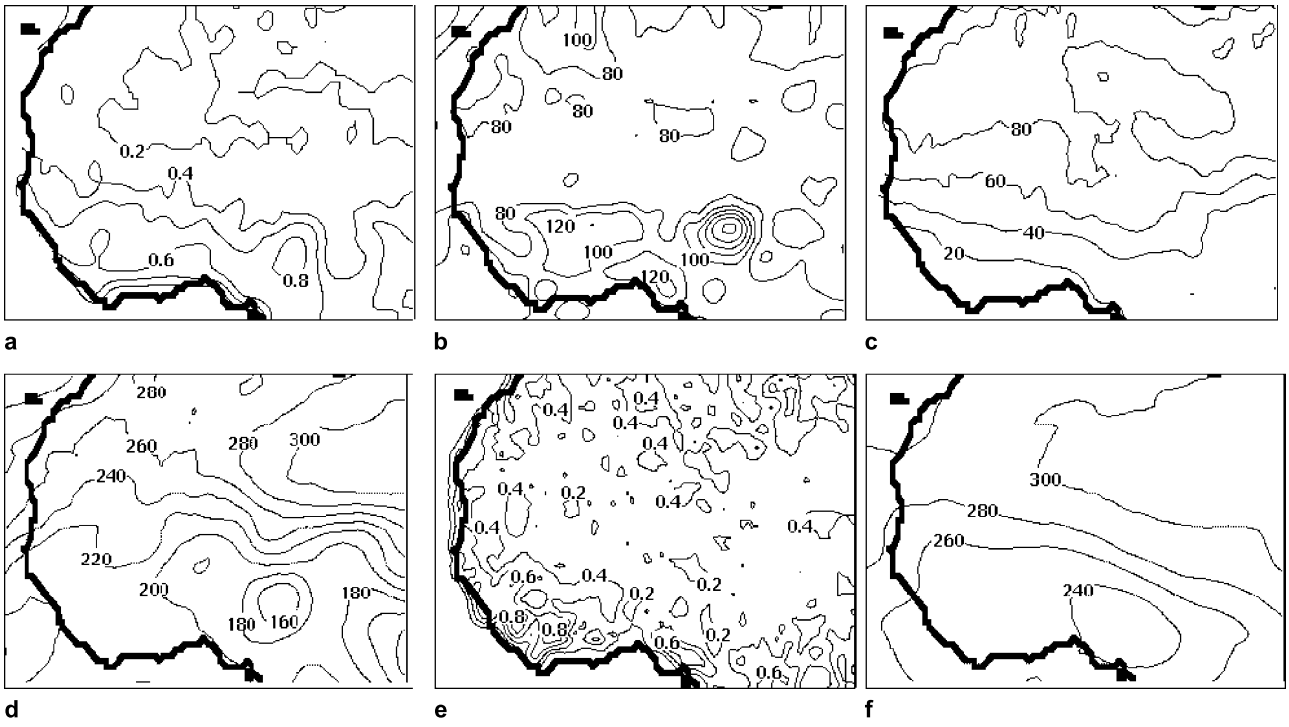

Fig. 8. JJAS mean fields, **a** RM2 soil moisture fraction, **b** RM2 upward latent heat flux at the ground, **c** RM2 upward sensible heat flux at the ground, **d** RM2 downward short wave flux at the ground, **e** RM1 soil moisture fraction, **f** RM1 downward short wave flux at the ground. Units of all fluxes are (Wm^{-2})

the coast. However, because of excessive surface winds (Fig. 2a), the RM1 maintained strong upward latent heat fluxes over most areas (not shown). The warmer Tg in the control are a consequence of some 40–60 Wm^{-2} additional downward short wave energy flux reaching the ground in the RM1 simulation (Fig. 8f), as compared to RM2 (Fig. 8d). The more sophisticated land surface treatment created more cloudiness in order to bring about the more realistic cooling between 6–10° N over West Africa. RM2 JJAS 1995 surface energy components were closer to NCPR values than in the control.

Figure 7b shows the latitude-pressure cross section of zonal winds along 0° longitude for the RM2 simulation, which should be compared to Figs. 2 and 5b. The zonal circulation over West Africa has been improved by the more realistic thermal structure. Monsoon westerlies are only slightly too strong and realistic vertical wind shear reverses the direction of the zonal circulation, creating an AEJ core of strong mid-tropospheric easterlies. This core is displaced some 5° southward of its NCRP position, as in the RM1 experiment with specified Tg. However, lateral wind shear north of the AEJ is more realistic for the RM2 outcome.

Figure 9a shows the JJAS 1995 mean precipitation distribution based on CMAP data. Maxima over 8° N, 13° W and 5° N, 8° E are joined by the zonal intertropical convergence (ITC) maximum running along 5–10° N. The JJAS mean for the control simulation (Fig. 9b) is oriented parallel to the core of AEJ zonal circulation (Fig. 3). The corresponding pattern in the prescribed Tg experiment (not shown) included an unrealistic swath lacking rainfall between 6–10° N over West Africa. RM2 mean JJAS precipitation (Fig. 9c) was not adversely affected by the colder Tg within 6–10° N, as in the RM1 Tg experiment. RM2 reproduced the observed maximum at 5° N, 8° E and gave realistic rates over West Africa westward to about 10° W. The more zonal orientation of the RM2 ITC maximum and its extention to the southwest coast are modest improvements over the control results. However, the RM2 did not simulate the more westerly maximum at the Atlantic coast, and there is still a conspicuous lack of precipitation where the Atlantic ITC is observed.

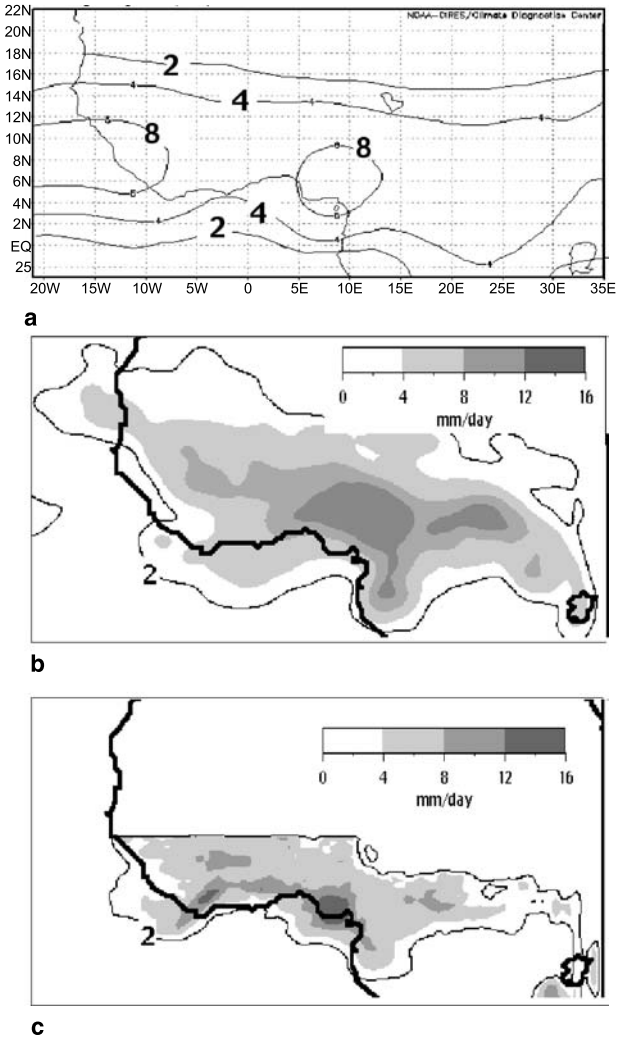

Fig. 9. Mean JJAS 1995 precipitation rates, **a** CMAP (courtesy CDC/NOAA), **b** RM1 control, **c** RM2

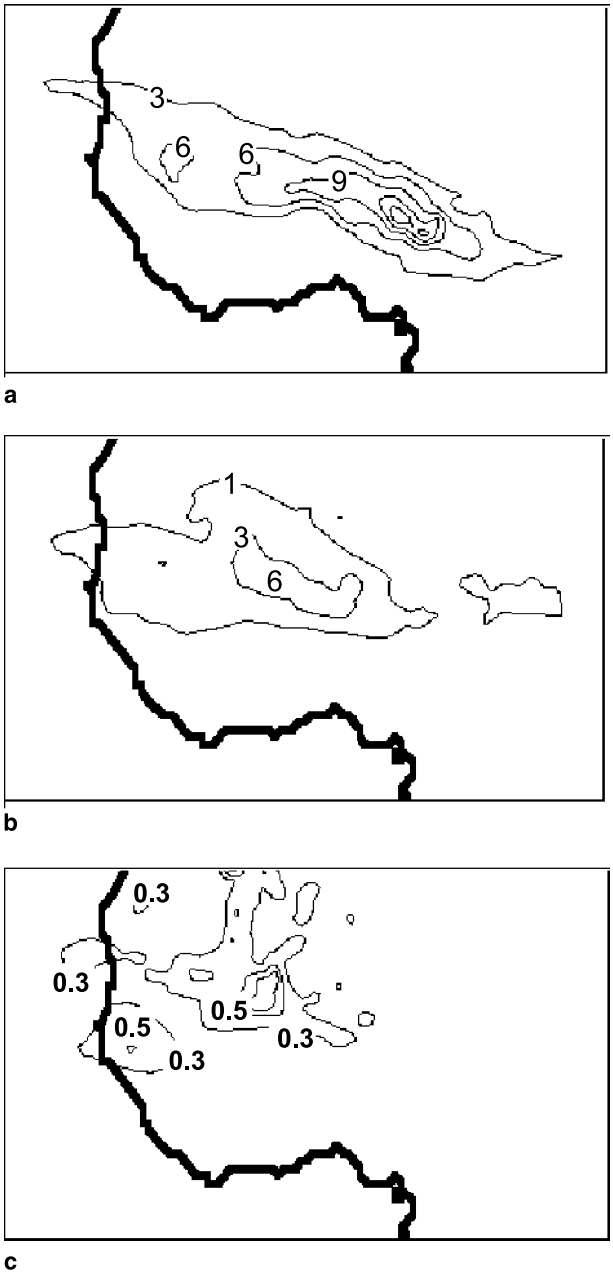

Fig. 10. Spatial distributions of vorticity variance ($\times 10^{-10}\,\mathrm{sec}^{-2}$) from time series of 700 mb vorticity, band pass filtered for 3–6 day periods; **a** control, **b** prescribed Tg experiment, **c** RM2

In summary, results show that the main correction to the original RM1 circulation field can be accomplished by making the distribution of ground temperatures more realistic over a rather narrow expanse of coastal land. The land process model accomplishes this correction and somewhat more, since it improves the simulation of ground temperatures throughout the domain.

3.4 AWD characteristics

A zone of maximum vorticity variance is created along a trajectory of transient cyclonic disturbances. Accordingly, Reed et al (1988) deduced AWD trajectories in gridded data from the ECMWF analysis and forecast archive projected on a 3° by 3° latitude–longitude grid by mapping the 700 mb vorticity variance filtered for 2.9–4.0 and 2.9–4.7-day periods. Their analysis was confined to August–September 1985 and it showed a northerly AWD track along 21° N as well as a more southerly one (12–15° N) very similar to the RM1 control results in Fig. 10a: variances of vorticity from time series band pass filtered for 3–6 day periods. Maxima are stronger than in Reed et al (1988), and one might

conjecture that this is related to the finer spatial resolution of the RM1. The belt of maximum 700 mb vorticity variance for the control simulation cuts a swath across West Africa from 9° N in the east to 19° N at the Atlantic coast. Maximum vorticity variance in the control occurs within the zone of highest lateral wind shear south of the core of maximum easterlies (see Fig. 3). The corresponding spatial distribution of 700 mb vorticity variance for the Tg experiment is shown in Fig. 10b. The maximum vorticity variance in this experiment is much lower than in the control, and it is displaced to the northwest of the control maximum. Note that the mean zonal circulation in this case (Fig. 6a) features considerably less lateral wind shear. In addition, AWD trajectories implied by the pattern are more zonal and roughly parallel to the simulated AEJ core of maximum easterlies. Figure 10c shows that the maximum vorticity variance of 3–6 day waves in the RM2 simulation is even weaker than for the prescribed Tg experiment. In fact, values here are comparable to those shown by Reed et al (1988) for the ECMWF analysis and forecast archive. However, the area of implied wave activity is further north, between 15–17° N, except at the coast where a weaker maximum is registered at about 13° N.

Composites of AWD characteristics were constructed from the JJAS RM simulations as follows. Events for a composite were chosen using four times daily 3–6 day period band pass filtered time series of the 700 mb meridional wind component (v7) at selected ''reference'' grid points. For each summer simulation, a subset of events was chosen as the average over all time steps for which v7 in the filtered time series was a maximum (minimum). It is assumed that an AWD structure was present immediately west (east) of the reference point during each such event. Composite averages of unfiltered simulated fields of precipitation and the 700 mb circulation for these selected time steps were constructed in each case.

Composite results based on several different reference points were quite similar. Figure 11a shows the control run precipitation and 700 mb circulation composite based on southerly maxima of v7 at 12° N, 0° and Fig. 11b shows the corresponding composite for the Tg experiment. Composite AWDs are positioned within the swath of maximum vorticity variance shown in

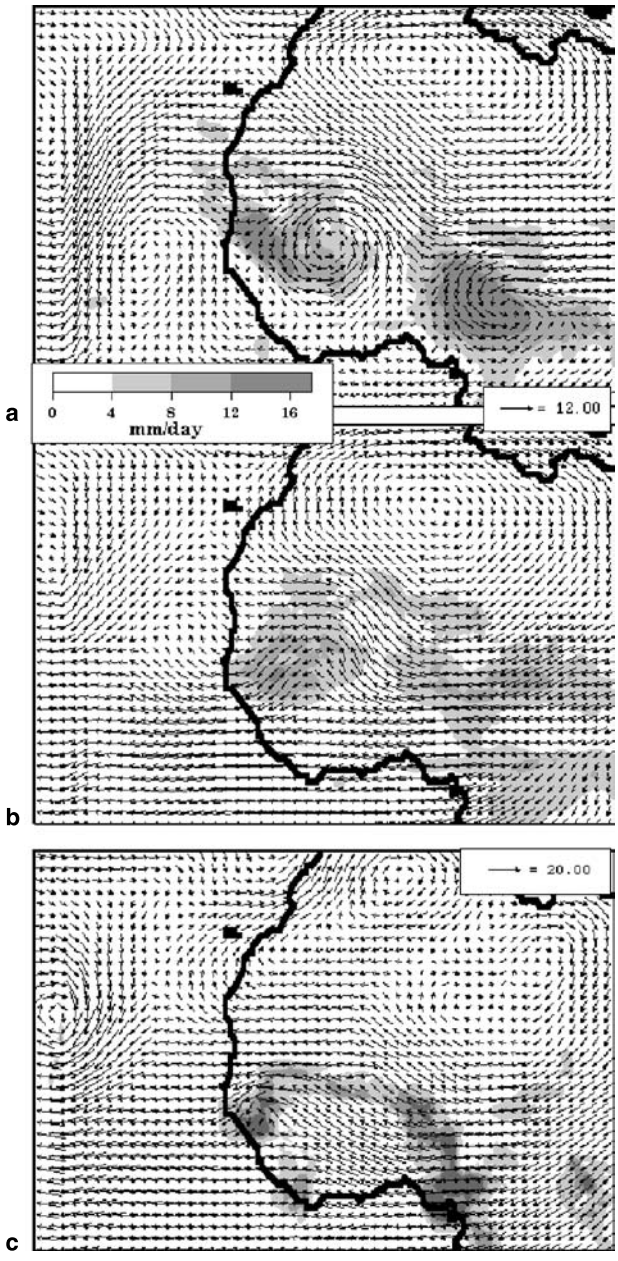

Fig. 11. Circulation at 700 mb and precipitation rates based on a maximum southerly wind at 12° N, 0°; **a** Control composite, **b** Prescribed Tg experiment composite, **c** RM2 on June 20th

Figs. 10a and 10b, implying that 3–6 day period oscillations in vorticity occur as the AWDs traverse West Africa on their westward trajectory to the Atlantic Ocean. The composite AWD for the control is a closed cyclonic circulation centered on 14° N, 4° W (hereafter AWD1). However, a second AWD (AWD2) is evident some 2000 km upstream (at 9.5° N, 13.5° E), indicating that AWDs routinely occurred at regular spatial

intervals representative of AWD wavelengths. These closed cyclonic circulations reflect the deep westerlies that reach 700 mb over southwestern West Africa (Fig. 3). The positioning of the AEJ core of easterlies along 8° N in the Tg experiment transformed its corresponding composite AWD into an open wave lacking westerly circulation and with the trough along 6° W (Fig. 11b). In addition, the Tg experiment results increased the separation between this composite AWD and the next upstream disturbance. In contrast to the 2000 km wave length, this experiment suggests wave lengths in excess of 3000 km, although the upstream AWDs are too close to the domain boundary to determine their exact location. A longer wavelength than in the control may be related to increases in the mean zonal (easterly) circulation at 700 mb, which, over the southern parts of the waves, approaches 6 ms^{-1} and/or to a slight increase in the periods of the AWDs.

The control composite features precipitation rates of >12 mm day^{-1} southwest of the AWD1 center of circulation. Similar rates associated with AWD2 cover a broader area, but they are centered within the same quadrant. Figure 11b shows that the AWD composite for the Tg experiment also organizes a precipitation maximum, although the maximum in the southwest quadrant is somewhat lower than for the control. The inhibition of precipitation recalled above for the Tg experiment is manifest by the relatively dry areas south of 10° N in Fig. 11b.

Wave amplitudes for the RM2 simulation were rather weak. Since the composite AWD is so shal-

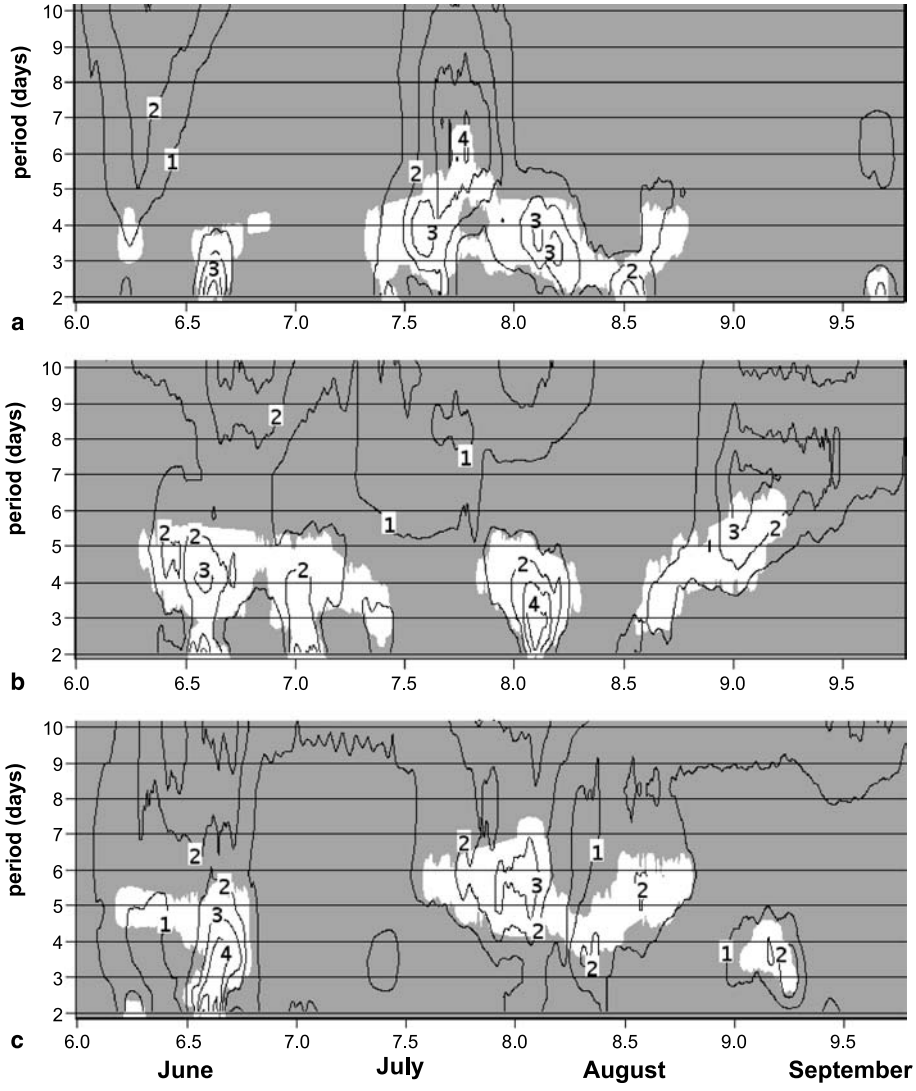

Fig. 12. Wavelet analyses of JJAS time series of the 700 mb meridional wind component at 12° N, 0°; **a** control, **b** prescribed Tg experiment, **c** RM2

low, Fig. 11c instead shows a single simulated AWD on June 20 at 12° W. The 700 mb circulation for the single time step describes an open wave with an imbedded line of maximum precipitation within the trough. As in the composites shown in Figs. 11a and 11b, this time step also coincides with a maximum in the 3–6 day filtered v7 time series at 12° N, 0°.

Wavelet analyses of v7 time series at the 12° N, 0° reference point are shown in Fig. 12. Note that based on Fig. 10c, this location is not a prime area of AWD activity for the RM2 simulation. Nevertheless, in all three cases, significant amplitudes occur during certain finite intervals, although not continuously throughout the summer. During the longest such interval in the control results, periods of 3–5 days are favored, but the dominant periodicity is still somewhat variable. Significant AWD activity in the prescribed Tg experiment (Fig. 12b) overlaps control results (Fig. 12a) but also occurs on different dates in July and September. Late July and August AWD activity in the RM2 (Fig. 12c) is at longer periods (4–7 days) than for the RM1. Note that there are several weeks of v7 variability in this simulation that include periodicities greater than six days. Such activity is not represented in Fig. 10c since vorticity variance was band pass filtered to include only 3–6 day periods. Note also that the June 20th AWD at 12° W shown in Fig. 11c is probably related to the strong wavelet signal first detected at 0° longitude on June 16, with periods ranging from 2–6 days.

Spectral analysis of v7 time series at the reference point (not shown) indicates that, while the dominant periods of AWDs in the control were about 3.5 days, in the Tg and RM2 experiments they were closer to 4.5 days and 5 days, respectively. Accordingly, the response to swifter propagation speeds seems to be increases in the periods and wavelengths. In addition, the spectral amplitude peaks at this reference point were only about 60% and 18% of the corresponding control value in the respective prescribed Tg and RM2 simulations. Figure 10 shows that some of this difference owes to the northward displacement of the AWD trajectories in the Tg and RM2 experiments, but even within the main axis of activity, the control was characterized by stronger AWD vorticity extremes and higher spectral amplitudes of 3–6 day period waves.

4. Discussion and conclusions

Simulation experiments over West Africa forced by JJAS 1995 NCRP data were made with two versions of a limited area climate model computed on a grid lattice with 0.5° spacing. The version used in previously published studies (RM1) computes soil moisture interactively with statistically based multivariate equations. Very strong, closed cyclonic disturbances in the RM1 simulation were found to be related to unrealistic features of the modeled thermal structure and circulation. In particular, the failure to sufficiently cool the ground by generating adequate cloudiness to intercept solar energy over the Gulf of Guinea coastal region had far reaching repercussions.

Unrealistic near-surface temperature gradients over West Africa in the RM1 control simulation created an accelerated westerly monsoon circulation which, combined with reduced vertical wind shear, produced a very deep layer of westerlies. The mid-tropospheric AEJ was displaced northward and artificially strong lateral wind shears created exaggerated vorticity maxima. Many of the RM1 discrepancies in seasonal mean fields were remedied by RM2, which incorporated a sophisticated land surface process model. RM2 yielded higher JJAS mean percentages of ground wetness over southwest Africa, which in turn created realistic evaporation rates and a more persistent cloud cover. These RM2 adjustments led to realistic ground temperatures and temperature gradients over West Africa. The RM2 modifications also corrected the overly deep layer of monsoon westerlies and produced an AEJ that better matched the corresponding observational analysis, even though core wind speeds were too high and the jet was too far south. More realistic mid-tropospheric lateral wind shear yielded more reasonable levels of vorticity variance. Detected AWD were low amplitude open wave disturbances, replacing the intense cyclonic storms of RM1.

To better understand the importance of the land surface treatment by RM2, an ad hoc RM1 experiment was made in which realistically cool ground temperatures were prescribed over West Africa between 6–10° N. Results demonstrated that most of the adverse features of the RM1 model simulation of both the mean summer climate and individual synoptic disturbances were related to discrepancies in modeled ground

temperatures along this particular, rather narrow swath of the West African coast. The study implies that the cooling effect of persistent cloudiness along the Gulf of Guinea coast prevents AWD from developing into more intense storms with heavier precipitation.

Acknowledgements

This research was supported by the National Science Foundation under grant no. ATM-0089563 and by the NASA Climate and Earth Observing System Programs. Helpful comments of Dr. Arona Diedhiou are gratefully acknowledged.

References

Burpee RW (1972) The origin and structure of easterly waves in the lower troposphere of North Africa. J Atmos Sci 29: 77–90

Deardoff J (1978) Efficient prediction of ground surface temperature and moisture with inclusion of a layer of vegetation. JGR 83: 1889–1903

Druyan L, Hall T (1996) The sensitivity of African wave disturbances to remote forcing. J Appl Met 35: 1100–1110

Druyan L, Lonergan P, Saloum M (1996) African wave disturbances and precipitation at Niamey during July–August 1987 and 1988. Climate Res 7: 71–83

Druyan L (1998) The role of synoptic systems in the interannual variability of Sahel rainfall. Meteorol Atmos Phys 65: 55–75

Druyan L, Fulakeza M, Lonergan P, Saloum M (2001) A regional model study of synoptic features over West Africa. Mon Wea Rev 129: 1564–1577

Folland C, Palmer T, Parker D (1986) Sahel rainfall and world-wide sea temperatures, 1901–85. Nature 320: 602–606

Fulakeza M, Druyan L, Krishnamurti T (2002) A simple soil moisture scheme for regional climate simulations in the tropics. Meteorol Atmos Phys 79: 105–126

Hansen J, Sato M, Nazarenko L, et al (2002) Climate forcings in Goddard Institute for Space Studies SI2000 simulations. J Geophys Res 107: 4347

Lamb P, Peppler R (1992) Further case studies of tropical Atlantic surface atmospheric and oceanic patterns associated with sub-Saharan drought. J Clim 5: 476–488

Lough J (1986) Tropical Atlantic sea-surface temperatures and rainfall variations in sub-saharan Africa. Mon Wea Rev 114: 561–570

Moustaoui M, Royer J-F, Chauvin F (2002) African easterly wave activity in a variable resolution GCM. Clim Dyn 19: 289–301

Pytharoulis I, Thorncroft C (1999) The low-level structure of African easterly waves in 1995. Mon Wea Rev 127: 2266–2280

Reed R, Norquist D, Recker E (1977) The structure and properties of African wave disturbances as observed during phase III of GATE. Mon Wea Rev 105: 317–333

Reed R, Klinker E, Holingsworth A (1988) The structure and characteristics of African easterly wave disturbances as determined from the ECMWF operational analysis/forecast system. Meteorol Atmos Phys 38: 22–33

Rosenzweig C, Abramopoulos F (1997) Land-surface model development for the GISS GCM. J Climate 10: 2040–2054

Taleb E-H, Druyan L (2003) Relationships between rainfall and West African wave disturbances in station observations. Int J Climatol 23: 305–313

Thorncroft C, Blackburn M (1999) Maintenance of the African easterly jet. Quart J R Meteorol Soc 125: 763–786

Authors' addresses: L. M. Druyan (E-mail: Ldruyan@giss.nasa.gov) and M. Fulakeza, Center for Climate Systems Research, Earth Institute at Columbia University, NASA/Goddard Institute for Space Studies, New York; P. Lonergan, Stinger Ghaffarian Technology, Inc., NASA/Goddard Institute for Space Studies, New York